Adaptation of the nuclear safety code CATHARE3 to supercritical helium flow

Sulayman Shoala, Christine Hoa, Eric Ercolani, Jean-Marc Poncet, Kim-Claire Le Thanh, François Dupouy, Roser Vallcorba, Benoit Lacroix, Sylvie Nicollet

Version of Record: https://www.sciencedirect.com/science/article/pii/S0011227520301375
Manuscript_8e5ea04cb6e941ef516d19b78f05cfd5

Adaptation of the nuclear safety code CATHARE3 to supercritical helium flow

Shoala Sulayman[a], Hoa Christine[a], Ercolani Eric[a], Poncet Jean-Marc[a], Le Thanh Kim-Claire[b], Dupouy François[b], Vallcorba Roser[c], Lacroix Benoit[d], Nicollet Sylvie[d]

[a] CEA, DRF/IRIG/DSBT

[b] CEA, DEN/DANS/DM2S

[c] CEA, DRF/IRFU/DACM

[d] CEA, DRF/ IRFM/STEP

Author mail address: sulayman.shoala@cea.fr

Abstract

Several international projects on nuclear fusion are in progress and comprise cryogenic systems for cooling components such as superconducting magnets. Different thermal-hydraulic codes already exist for sizing and validating these cryogenic devices. However, there is still no qualified scientific calculation tool to perform safety thermal hydraulic analyses encountered in fusion reactors. For this purpose, we have started the adaptation of the CATHARE system code, the reference thermal-hydraulic tool for safety studies of French Pressurised Water Reactors developed by CEA, EDF, Framatome, and IRSN, to model supercritical helium flows. Properties of supercritical helium were already available in CATHARE with the fluid library REFPROP. We implemented suitable correlations for friction factors and heat transfer coefficients to account for specific hydraulic parameters of helium flow in Cable In Conduit Conductors (CICC) that are used in superconducting magnets. Then, we performed first evaluations of the CATHARE code abilities to model thermal-hydraulic transient in cryogenic devices of a tokamak. Two cases of helium flow in a CICC of a JT-60SA toroidal field coil have been studied, and comparisons were performed with experimental data and the THEA code developed by CryoSoft. Simulations focusing on the behaviour of a device protected by a safety valve against incidental pressure increase were also performed. CATHARE results were compared with available experimental data on supercritical helium discharge through the safety valve of a tank in case of failure of the insulating vacuum.

Keywords

Fusion
JT-60SA
Cable In Conduit Conductors
Safety Valve
Discharge Line

1 Introduction

Several international projects on nuclear fusion are in progress and involve building new tokamak reactors, for instance JT-60SA in Japan and ITER in France. To produce and control the nuclear fusion reaction in the tokamak, essential equipment such as superconducting magnets are operated at very low temperature and cooled around 4 K with forced flow supercritical helium. A cryoplant produces the cooling power and the supercritical helium is distributed through a complex system of cryolines that make up the cryodistribution system.

Different thermal-hydraulic codes have been developed for sizing and validating the design of the magnets and their cryodistribution. Nevertheless, there is still no qualified scientific calculation tool to perform safety thermal-hydraulic analyses on accidental transients encountered in fusion reactors. Indeed, these cryogenic circuits are components of a nuclear installation and can be in contact with radioactive elements. Studies have to be carried out to demonstrate the nuclear safety of the installation to the authorities. These investigations can be

based on the use of qualified scientific calculation tools. For a scientific calculation tool to be recognized as qualified, it needs to provide sufficiently reliable results to demonstrate nuclear safety. This recognition is established after verifications, validations, uncertainties quantification and transposition processes, in order to certify that the calculation tool is able to calculate quantities of interest with the uncertainties adapted to the needs and in the field of use.

A qualified tool to perform calculations of thermal-hydraulic transients in actual nuclear fission reactors already exists. The CATHARE system code is currently the reference thermal-hydraulic tool for safety studies of French Pressurised Water Reactors (PWR) [1]. Developed since 1979, it has been thoroughly validated for modelling two-phase water flow with respect to a dedicated experimental program in a collaboration between CEA, EDF, Framatome, and IRSN. While the CATHARE code was first dedicated to model water applications, some other fluids can now be used.

In this paper, we propose to perform some initial evaluations of the capabilities of the CATHARE code to model thermal-hydraulic transient scenarios in supercritical helium flow encountered in fusion reactors. Two different applications related to the safety of cryogenic circuits of a Tokamak have been investigated. The first modelling part concerns the Cable In Conduit Conductors (CICC) of a JT-60SA Toroidal Field coil. Additional correlations have been implemented in the code to perform thermal-hydraulic calculations of supercritical helium flow in a cable of a superconducting magnet. Then, a pure hydraulic experimental test performed on a coil has been modelled with the CATHARE code to carry-out a primary validation of the model. A comparison with the THEA code [2] has also been realised on a case of a high heat load deposition on the cable and the discrepancies between the two codes were investigated. The second modelling part focuses on the protection of cryogenic facilities by a safety valve against incidental pressure increase. An experimental device [3] has been modelled in the CATHARE code and results were compared with available experimental data on supercritical helium discharge through the safety valve of a tank in case of failure of the insulating vacuum.

2 The CATHARE CODE

2.1 General description

CATHARE-2 is the current industrial version of the code, although it will be progressively replaced by CATHARE-3, the current development version of the code [4] and the one used in this work. The CATHARE code use a two-phase and six-equation model [5] with additional equations for non-condensable gases and radio-chemical component transportation. This model is based on the average mass, momentum and energy equations for each phase over the cross section A and the time t. The 6 main hydraulics variables are the pressure, the void fraction, enthalpies and velocities of each phase. With this model, the CATHARE code can consider all thermal and mechanical disequilibrium between phases. The equation system is closed thanks to closure laws [6] that take into account the different flow regimes, heat and mass transfer between phases or between fluid and walls. These correlations are extracted from the literature or from experimental data [7].

In addition, it is a modular code. Each hydraulic circuit is modelled by assembling volumes (0-D), axial pipes (1-D), and three-Ds (3-D) hydraulic modules. Sub-modules are also available to represent thermal and hydraulic components such as thermal walls, heat exchangers, pumps, valves, pure energy or fluid sources and sinks. The numerical scheme uses the finite volume method for mass and energy equations, and the finite difference method for the momentum equation [8]. A staggered grid is used for the spatial discretisation, with velocities calculated on the face of each mesh and other hydraulic variables on the scalar point located at the middle of the mesh. Temporal discretization is implicit for the 0-D and 1-D module, and semi implicit for the 3-D module. The non-linear system is solved with the Newton-Raphson iterative method.

In this study, as only monophasic supercritical helium is considered, CATHARE-3 is used with monophasic calculations [9]. Development for monophasic simulations mainly consists in reducing the six standard balance equations to three balance equations for the gas phase only and insure compatibility with the different modules and sub-modules. The benefits of using single-phase flow calculation are a shorter computing time and a better convergence of the results. Moreover using different fluids than water is possible through the coupling with the Reference Fluid Thermodynamic and Transport Properties Database (REFPROP) developed by the NIST [10]. REFPROP can compute properties of more than 100 fluids and enables the use of real gas properties. CATHARE-3 can access fluid properties available in REFPROP database through the EOS component [9], which is developed by the CEA to link thermal-hydraulic codes and fluid property database.

2.2 Validation methodology of the code

To perform safety studies, a numerical calculation tools has to be validated. The validation of the CATHARE system-scale code and its physical models is carried out in several steps, each corresponding to a different validation scale [1] [7]:

- The first step is the verification of CATHARE results on Separate Effects Tests (SET). Experimental facilities are developed to study a particular physical phenomenon and are modelled with the code. Experimental data is compared to the code prediction to validate a physical model and quantify uncertainties.
- The second step is a system scale validation on Integral Effects Tests (IET). It is also based on a comparison between experimental and CATHARE results. A wide range of normal and incident transient scenarios are carried out on experimental facilities that represent a part or a whole reactor. The aim is to verify the abilities of the code to consider the coupling between the different physical phenomena.

Once the set of tests has been carried out, new correlations are integrated into a version of the code identified by a version number. The code is then validated, which means that physical phenomena are computed well in the defined physical domain. Currently, the CATHARE code is validated only for water flows in the pressure and temperature range encountered in normal or accidental operation of a PWR. The long-term objective is to follow the validation methodology for supercritical helium. To start the validation process, benchmark tests with other thermal hydraulic codes and preliminary experimental comparisons have been investigated.

3 First analysis: dynamic thermal-hydraulic modelling of Cable in Conduit cable of JT-60SA TF Coils

3.1 Description of the thermal-hydraulic model for CICC

The Toroidal Field (TF) system of the JT-60SA Japanese tokamak is composed of 18 Nb-Ti superconducting coils [11]. A TF coil consists in a winding pack (WP) of 6 Double Pancakes (DP). Each DP is stack-wound in 6 turns and inserted into a stainless steel casing (Figure 1). One Pancake consists of a 113 m long Cable-In-Conduit Conductor (CICC) made of superconducting strands wrapped in a 2 mm thick stainless steel jacket, which is then surrounded in a 1 mm thick G10 insulation. The TF CICC constitutes a single channel with a 18mm*22mm cross-section containing a bundle of 324 Nb-Ti strands and 162 copper strands [12]. Figure 2 shows the cross section of a JT-60SA TF coil (TFC) CICC and Table 1 gives its reference hydraulic characteristics. The CICC is cooled by a forced circulation of supercritical helium through the interstices between the strands. This configuration maximizes the contact area between the cryogenic fluid and the superconducting strands. It ensures efficient cooling of the strands and better thermal stability against disturbances. Additional helium channels in the stainless steel casing improve the cooling of the structure.

CATHARE-3 is not yet able to take into account electrical laws in the strands. To perform the first evaluation of the code ability in the modelling of supercritical helium flow, it was decided to not consider electric phenomena in the CICC. Nevertheless, hydraulic configurations encountered in these cables are quite far from the case of a pipe and requires specific correlations to calculate the pressure drop and heat exchange transfer between the fluid and the structures in the conductor. For this reason, specific correlations to CICC available in the literature have been implemented in CATHARE-3 to model helium flow through the bundle of superconducting strands.

Parameter	Value
Outer/Inner Jacket dimensions	26 x 22/22 x 18 mm
Strand o.d.	0.81 mm
Nb. Str.	486
Helium Area A_W	125.8 mm²
Wetted perimeter P_w	1.10802 m
Hydraulic diameter D_h	0.454 mm
Pancake Length L_p	113.28 m

Table 1 Conductor Hydraulic Reference Data

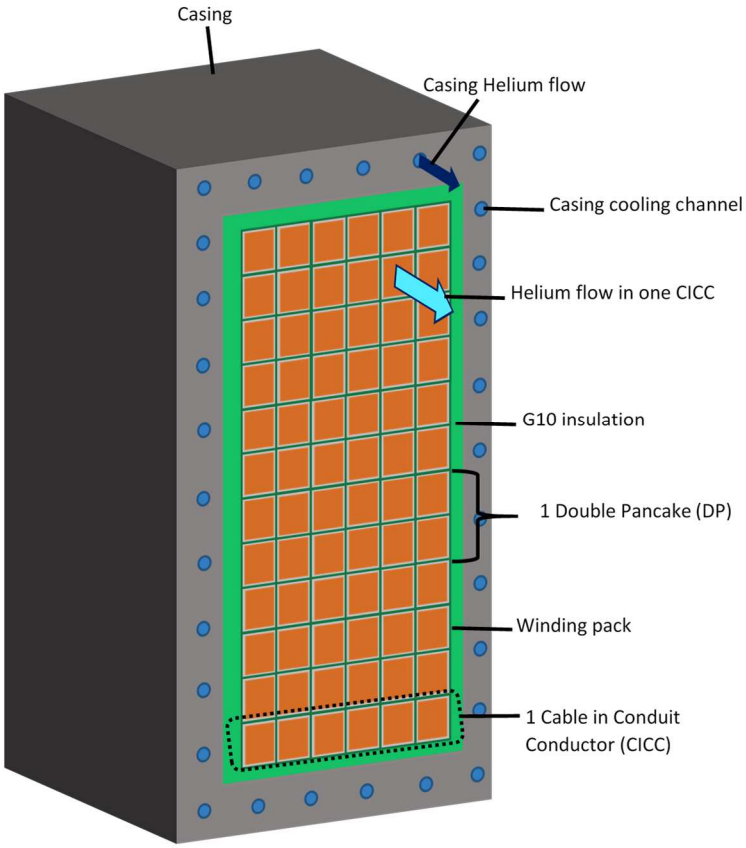

Figure 1 Cross section of a TF coil

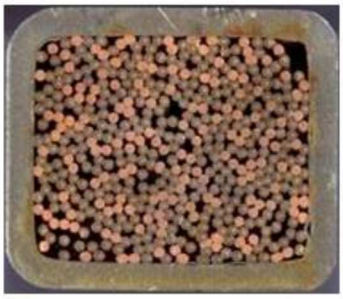

Figure 2 JT-60SA TF CICC cross section (courtesy of F4E)

Two correlations have been implemented to calculate the pressure drop in the CICC. The first one is the Darcy-Forchheimer correlation and is based on a porous media analogy [13]:

$$f_{bundle} = \varphi^2 C_F \frac{D_h}{2K^{0.5}} + \varphi \frac{{D_h}^2}{2K} \frac{1}{Re} \quad (1)$$

$$K = K_0 \frac{\varphi^3}{(1-\varphi)^2}$$

$$\frac{C_f}{\sqrt{K}} = \frac{C_0}{\varphi^n}$$

With K the cable permeability, C_F the drag factor and φ the void fraction. The multiplying constants K_0 and C_0 are given in Table 2. They depend closely on the strands arrangement in the CICC and have been calculated in [13] to obtain the best fit with datasets.

Due to the large dependence of the pressure drop on the cable geometry, scattering of the hydraulic characteristics of the different DP were detected during tests [14]. JT-60SA conductor samples used in the manufacture of the different TF coils have been extracted directly from the production line and tested with the OTHELLO test facility [15]. From these measurements, the friction factor depending on the Reynolds number Re was determined for each DP with the best fit according to the formula:

$$f = \alpha + \beta\, Re^{\gamma} \qquad (2)$$

With α, β and γ measured for each DP tested. For the moment, the correlation is available in the code only for one DP used in the manufacture of a certain TF Coil (DP1 of the coil TFC02). Physical constants used for this case are given in Table 3.

The heat transfer coefficient between the helium flow and solid elements of the cable (strands and stainless steel jacket) is calculated with the Nusselt number Nu from the Colburn analogy (3), which allows determining the heat transfer as a function of the fluid friction factor f deduced from (2) [16].

$$Nu = \frac{f}{2} RePr^{\frac{1}{3}} \qquad (3)$$

With Pr the Prandtl number.

The heat conduction through the material is calculated by CATHARE-3 in the 1-D direction perpendicular to the fluid flow by solving the heat conduction Fourier's equation (4), with $\dot{Q}$ the internal heat generation that is equal to zero in this case:

$$\rho\, C_p \frac{\partial T}{\partial t} = \nabla(\lambda \nabla \mathrm{T}) + \dot{\mathrm{Q}} \qquad (4)$$

This equation is implicitly coupled with the fluid equation through the thermal heat flux. CATHARE-3 is able to consider multi-layer wall with different material properties for each layer. The axial conduction is neglected.

Parameter	Value
K_0	19.6×10^{-9} m^2
C_0	2.42 m^{-1}
n	5.80

Table 2 Coefficients of the friction factor used in the Darcy-Forchheimer correlation

Parameter	Value
α	0.089743
β	50.876958
γ	-0.781075

Table 3 Coefficients of the friction factor of the Double Pancake 1 of the TFC02

3.2 Modelling of an experimental thermal-hydraulic test on a JT-60SA TF Coil

3.2.1 Description of experimental test

Before their delivery to Japan and their integration in the tokamak, the performance of each of the 18 TF coils of JT-60SA was checked. A dedicated device, called Cold Test Facility (CTF), was set up at CEA Saclay [17]. The evaluation of each coil was carried-out in 4 steps [18] [19]. First, the coils were tested at room temperature during the "Warm test" to perform conformity assessment such as resistance measurement, insulation and leak tests. Then, the coils were cooled down to carry out experiment at nominal temperature of 5 K without electrical power, followed by analysis with coils energized at the nominal current of 25.7 kA. During this last testing sequence, quench tests were performed to check the temperature margin against a quench scenario, which consists in the transition of a conductor from superconducting to normal resistive state. These first experiments allowed checking some performances of TF coils of JT-60SA concerning thermal-hydraulic and electrical characterization. Experimental results have been analysed and several coupled physical phenomena which

influence the quench dynamic have been identified [20] [21]. To complete these analyses, additional studies based on numerical simulation of quench cases observed experimentally were also performed with the dedicated THEA code [22] [23].

This part focus on an additional experiment also conducted on one JT-60SA TF Coil. Contrary to other tests, the objective is not the acceptance of the TFC but to provide experimental data to validate thermal-hydraulic codes. The studied transient consists in an inlet temperature pulsed scenario without electrical current in the cable. In practice, operators control the helium temperature with an electrical heater located at the inlet of the TFC. The associated analysis is thus only thermal-hydraulic. The mass flow in the CICC is maintained at 4 g/s from the beginning of the transient to t=3400s.

The heat input scenario is:

- Fast ramp from 4.75 K to 6 K inlet temperature.
- Wait until stabilization of the helium temperature (in a range of 0.1 K averaged over 180 seconds) and in any case not longer than 60 minutes.
- Fast ramp down to 4.75 K inlet temperature until stabilization

The supercritical helium flow in the casing is kept constant at 10 g/s.

3.2.2 Model description

A model of a single pancake of the JT-60SA TFC has been developed in CATHARE-3 (Figure 3). The conductor is modelled with the 1-D module thanks to the hydraulic characteristics given in Table 1. To simplify, only one pancake has been considered. Indeed, 2D effects and the coupling with the casing cooling channels have been neglected as shown in [24]. The friction factor is computed with the correlation (2) and the heat exchange between fluid and the thermal components (Nb-Ti/Cu strands, stainless steel jacket and impregnated G10 insulation) is calculated with the Colburn-Reynolds analogy (3). The transverse heat conduction (4) is considered, so each section of the CICC is thermally coupled with the flow of the previous and the next winding. The coupling is calculated by solving the heat conduction equation (4) through two layers of steel jacket (2mm thick each) separated by 2mm of G10 insulation. To simplify the model, the exchange area for the inter-turn thermal coupling is the same for each turn and corresponds to $1/6^{th}$ of the total external area of the pancake. Boundary conditions in the model are in line with the experimental operating conditions, with imposed inlet helium temperature, inlet and outlet pressure (Figure 4). The static heat load received by the winding pack is simulated by applying to the fluid a constant linear heat flux of 0.023W/m. The value of the heat flux was calculated from experimental data by performing an internal energy balance on the coil at the initial time. In order to evaluate the influence of the inter-turn thermal coupling, a comparison has been made with a calculation without inter-turn coupling. A THEA calculation was also performed with the same model to compare the results of both codes.

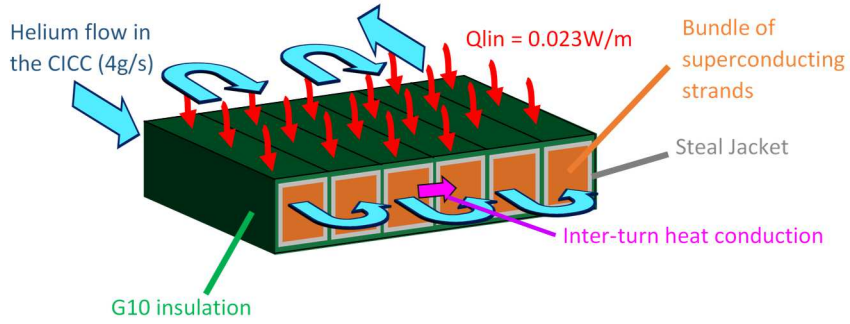

Figure 3 CATHARE-3 model of a JT-60SA TFC CICC with inter-turn coupling

3.2.3 *Results and analyses*

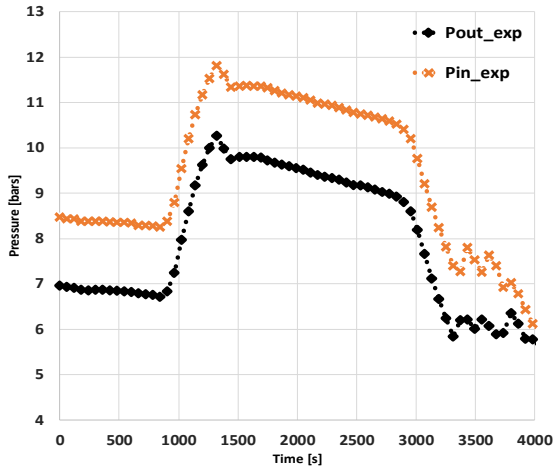

Figure 4 Inlet/Outlet pressure

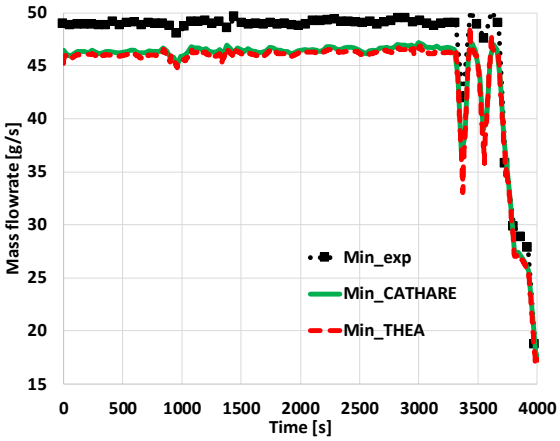

Figure 5 Inlet mass flow rate computed by THEA and CATHARE

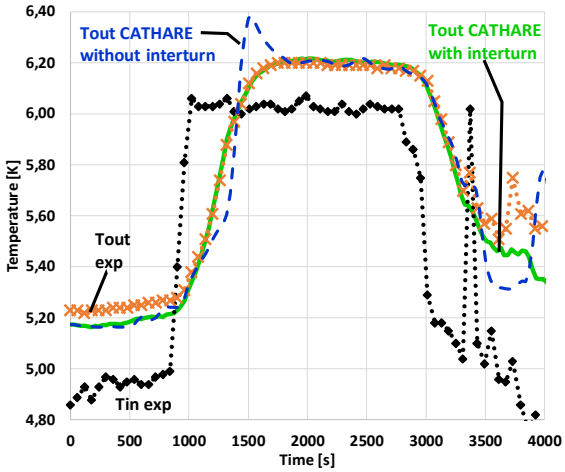

Figure 6 Tout computed by CATHARE with and without inter-turn heat transfer

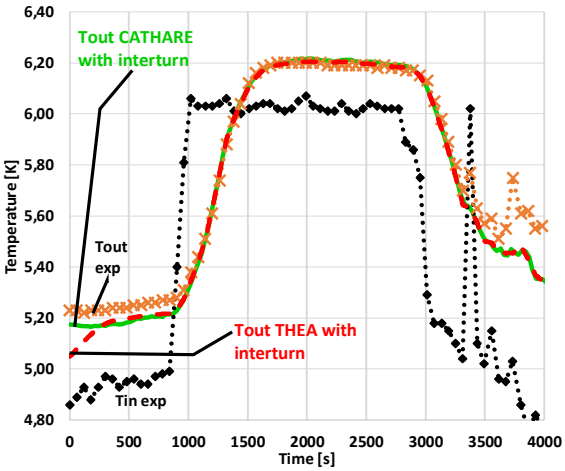

Figure 7 Tout computed by THEA and CATHARE with inter-turn heat transfer

The helium flow is due to the pressure difference between the inlet and the outlet of the CICC (Figure 4) imposed in the model as boundary conditions. In Figure 5, we observe that CATHARE-3 and THEA give very close values for the mass flow rate with a mean and a maximal relative difference which are respectively of 0.76% and 2% at t = 3930s. The total mass flow experimentally measured in the TFC is compared with 12 times the value computed by the two codes for one single pancake (6 Double Pancakes for one coil) and is on average 6% higher. The difference between experimental and numerical results can be explained in different ways, as uncertainties on experimental measurement or by the use of an empirical correlation to determine the friction factor. Indeed, as specified in 3.1, this correlation was established with measurement performed on one DP of a JT-60SA's TFC. As the experiment was not realised with the same coil, deviation can be observed.

The outlet temperature computed by CATHARE-3 with and without transverse heat conduction is shown in Figure 6. It highlights the necessity of considering the transverse heat diffusion through the inter-turn insulation to model correctly the outlet temperature variation. If this phenomenon is neglected, the shape of the computed outlet temperature is different from the experimental measurement, with a comparable slope as the one for the inlet temperature increase. This profile is consistent with heat propagation in the CICC due to pure advection of the warm front of helium, and the delay between the inlet and outlet temperature increases corresponds to the time needed by helium for flowing through the entire cable. For the CATHARE-3 simulation with the inter-turn model, the outlet temperature profile is close to the experimental one. The characteristic time of the transverse heat conduction is well evaluated by the code.

Except during the first 350s, THEA gives an outlet temperature similar to the one simulated by CATHARE-3 all along the transient (Figure 7). The gap observed at the beginning of the simulation is only due to difference in the initialization of the calculation in the two codes. In CATHARE-3, the transient does not start directly from the initial state defined in the dataset. A procedure determines a new steady state by taking into account

boundary conditions. The consequence is that the CATHARE-3 transient starts from a state which already considers the influence of the linear heat flux and the Joule-Thomson effect. On the other hand, THEA starts the transient with a constant temperature in the cable and 350s is the necessary time to reach the same state than CATHARE-3. Between 3500s and 4000s, small instabilities on the experimental outlet temperature are not reproduced by both codes. This difference with experiment has been identified as a consequence of not considering the helium supply circuit and so potential effects of valve openings by the operator at the end of the transient cannot be reproduced.

3.3 Heat load on a JT-60SA TF coil

One major safety case on superconducting magnets is the quench event. During a quench, the superconducting coil enters locally in the normal resistive state. Due to the high current level (26 kA), when the quench is triggered a large amount of Joule effect energy is dissipated and causes an important rise of temperature in the conductor. This local hotspot expands due to the heat conduction in the material. It provokes locally both temperature and pressure increase in the helium flow which can lead to backward-flow in the CICC. To avoid mechanical damage on the magnet, the quench must be detected quickly after its occurrence. Two different methods are used to insure the detection. The primary system is based on voltage measurements to detect abnormal electrical resistance, while the second one uses measurements of hydraulic signals such as the inlet and outlet flows of the TFC.

Quench ignition and propagation is a complex multi-physical phenomenon with strong couplings. Different works have been made with THEA to give a more comprehensive knowledge about the different phenomena that drive the quench ignition and propagation along the coil [22] . CATHARE-3 is not yet able to simulate all the physics in a quench as it does not include the electrical laws in the strands. However, the code is able to model a helium flow in a CICC and a comparison was realised to compare CATHARE-3 with THEA on a case of a local heat power injection in a JT-60SA TFC cable. As the CATHARE-3 is dedicated to perform safety studies, this article focus on two safety issues of quench ignition with the prediction of the hot spot temperature and hydraulic signal variations. Potential differences with THEA's results are investigated.

3.3.1 Model description

For this comparison, a 100 m long JT-60SA TF CICC has been modelled with hydraulic characteristics given in Table 1. To ensure the relevance of the comparison, datasets used in each code are equivalent. As we are only interested in hydraulic phenomena, the thermal power is directly applied to the fluid. It is done from 15 m to 25 m of the CICC inlet and its time profile is given in Figure 8.

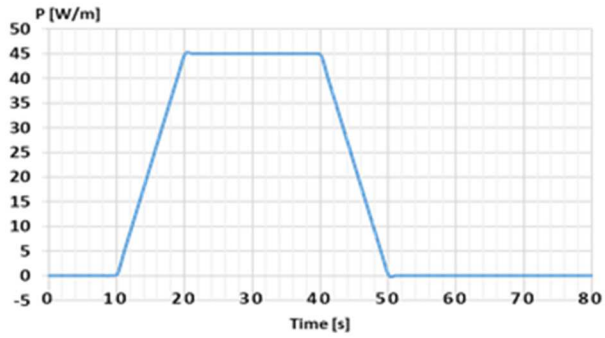

Figure 8 Thermal power injected in the helium flow

In both codes, the friction factor is calculated with the Darcy-Forchheimer correlation with a porosity of 0.32. The CICC is modelled by a 1-D object with 10 000 meshes and a maximum time step of 0.01s in order to ensure convergence in mesh and time of both models. Boundary conditions are given in Table 4 and stay constant during all the transient phase.

Parameter	Value
Inlet Pressure	6 bar
Outlet Pressure	5 bar
Inlet Temperature	4.5 K

Table 4 Boundary conditions on the CICC

3.3.2 *Results and analyses*

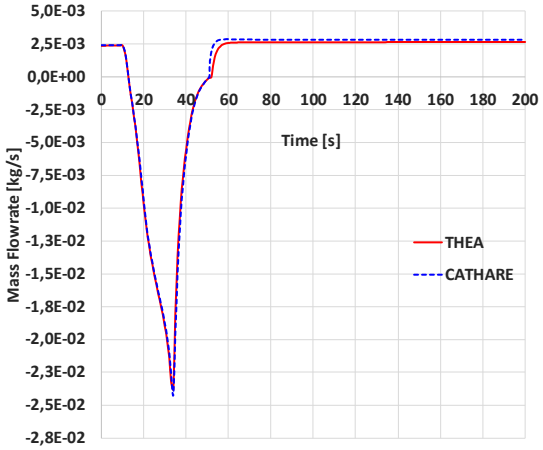

Figure 9 Inlet mass flow rate computed by THEA and CATHARE

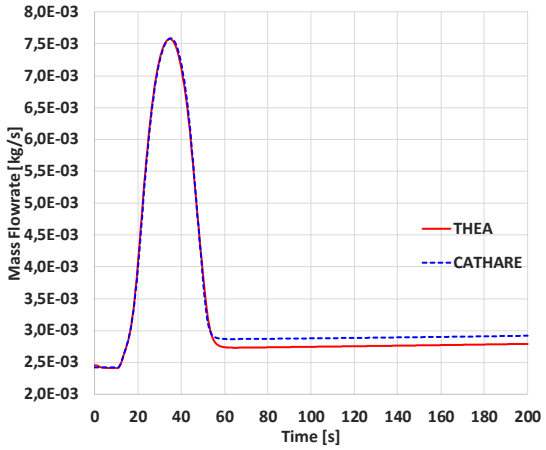

Figure 10 Outlet mass flow rate computed by THEA and CATHARE

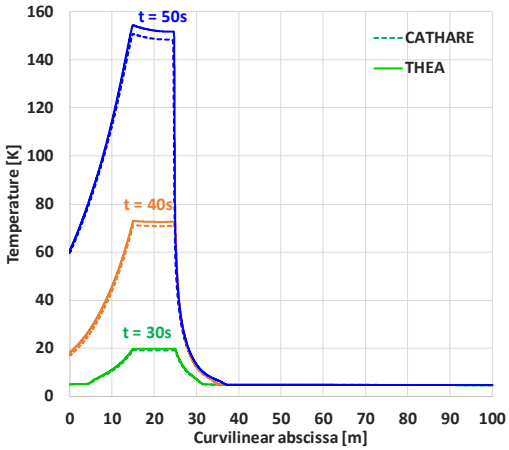

Figure 11 Temperature profile computed by THEA and CATHARE through the CICC during the heat power injection

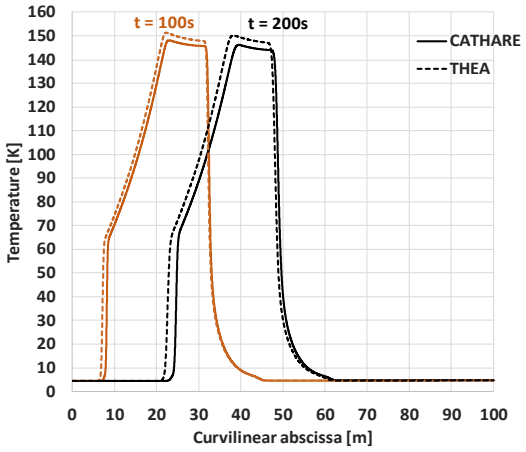

Figure 12 Temperature profile computed by THEA and CATHARE through the CICC during the advection phase

The transient state can be divided in three different phases, with an initial steady state from the beginning to t=10s, the heat power injection phase between t=10s and t=50s, followed by the advection of the hot helium wave along an adiabatic CICC until the end of the calculation (t=200 s). Each phase has its own dynamics.
The first phase is the nominal steady state imposed by the boundary conditions before the heat power injection. At this moment, the mass flow rate depends only on the pressure drop through the cable and the temperature increase of the fluid is driven by the Joule Thomson effect. Both codes compute similar flow conditions before the start of the pulse. The highest relative difference between the two codes is located at the CICC outlet and is about 0.4% on the mass flow and 0.1% on the fluid temperature.

The second phase starts at t=10s with the heat power injection. In the same way as a quench ignition, the energy received by the fluid causes local increase of temperature and pressure. Due to the fluid expansion, this hot spot spreads along the cable and leads to a backward-flow in the CICC. Figure 9 and Figure 10 show respectively the inlet and the outlet helium mass flow computed by THEA and CATHARE-3. Both codes predict variation of the inlet and outlet mass flow, respectively one and two seconds after the start of the hot spot ignition. Mass flow fluctuations computed by each code are in good agreement throughout the heating phase. The maximum backflow is reached at the same time in both codes and the relative difference on the peak value of the mass flow is 1.7%. The results of the two codes are closed, so CATHARE-3 is in good agreement with THEA on the prediction of thermal-hydraulic signal evolutions following the hot spot ignition. Concerning the temperature increase, Figure 11 gives the temperature profile along the CICC at different times of the heating phase. The same width of the temperature peaks indicates that the velocity of the warm helium front in each direction of the CICC is the same in both models, which is consistent with observations made on mass flow evolutions. Nevertheless, the hot spot temperature increases slightly faster in the THEA model. At the end of the heating phase, the relative difference on the hot spot temperature is 2.3 %, which represents 3.6 K. As CATHARE-3 and THEA predict the same physical phenomena with identical dynamics, it is difficult to judge the difference between both values of maximal hot spot temperature. Indeed numerous effects such as difference in the numerical scheme or in the convergence criteria can influence the results. One reason can be the difference on the helium characteristics databases used in each code. As CATHARE-3 used the REFPROP database which differs from the THEA one, the difference on the constant pressure heat capacity can reach 15% on the temperature and pressure ranges of the simulation.

The third step of the transient starts at t=50 s at the end of the heat power injection so the flow is again adiabatic. The back flow stops one second earlier in the CATHARE-3 model (Figure 9). When the mass flow through the cable is stabilized, a higher value of 0.15g/s is computed by CATHARE-3. Figure 12 shows the temperature profile along the CICC at different time of the advection phase. The displacement of the hot helium wave corresponds to a pure propagation phenomenon by the helium flow through the CICC. The warm helium area is moving a little bit faster in CATHARE-3 simulation than in THEA's results.

3.4 Conclusion on the modelling of JT-60SA TF coils by CATHARE-3

These two studies of a CICC in a JT-60SA TFC show that CATHARE-3 is able to model thermal-hydraulic phenomena in the bundle region of superconducting strands.

For the first study, the modelling of an experimental thermal-hydraulic test shows that the correlations are well implemented and provide consistent results. The effect of the inter-turn coupling along the conductor has been well reproduced and therefore the calculated outlet temperature profile fits well the experimental data.

The second study is a benchmark on a CICC configuration without electrical current but with a high heat injection to create a situation closed to quench ignition. Good agreements were obtained between CATHARE-3 and THEA. CATHARE-3 has demonstrated its ability to predict the same evolutions as THEA concerning back flow and thermal hydraulic responses at the hot spot ignition. Some differences on the hot spot temperatures have been identified and could be explained by discrepancies on the helium property databases of the two codes.

4 Second analysis: dynamic thermal-hydraulic of a safety valve line

4.1 Safety Valve Sizing

One of the major risk with liquid helium vessel in a cryostat and liquid helium storage is a failure of the insulating vacuum. Due to the large temperature differences with the ambient atmosphere, the fluid inside the tank receives important heat flux when the insulating vacuum is lost. Due to helium low heat of vaporization and large difference of density between gas and liquid, the pressure inside the helium vessel would increase significantly during a failure of the insulating vacuum. For example, 1 L of liquid helium expands to 780 L of gas at room temperature and atmospheric pressure. In order to avoid incidents, liquid helium vessels have to be protected with sufficiently large safety valves.

The safety valve is sized in order to evacuate a sufficient helium mass flow to guarantee that the maximum pressure remains below a set maximum value. The mass flow that must be expelled is proportional to the heat flux received by helium. Therefore heat transfer between the cryogenic fluid and the atmosphere of the broken vacuum chamber has to be known and quantified. Several experimentations were carried-out to provide data for the sizing of safety valves. In his experience, Lehmann measured a 3.8 W/cm² heat flux received by liquid helium at a constant pressure of one bar [25]. This value is actually the reference for sizing safety valves, but the CEA Grenoble [3] and the Karlsruher Institut für Technologie (KIT) [26] have also performed some measurements for supercritical helium. Indeed, as supercritical helium remains a monophasic fluid, heat transfer mechanisms differ from those with liquid helium which can boil. The CEA team measured a heat flux of 1.85 W/cm² transmitted from the inner wall of the tank to supercritical helium while KIT obtained a value of 1.75 W/cm² between the external wall of the cryogenic vessel and the venting fluid.

These reference values could be used in a future European standard on the sizing of safety valves for helium facilities. Knowing the value of the heat flux received by the fluid, it allows calculation with 0-D model of the mass flow to be evacuated from the tank to keep a constant pressure. This estimation is sufficient to size a safety valve directly located on the tank, but suffers from solver simplification in the case of a distant safety valve connected to the tank by a discharge line. Indeed, the discharge line is not necessarily insulated and the helium can received additional heat flux along the discharge line. Moreover, geometrical effects can have additional impacts on the pressure drop or on the accumulation of mass in this additional volume. As this entire phenomenon is a severe transient scenario, it is difficult to quantify the discharge mass flows with analytical models. A solution proposed by CEA for evaluating the impact of each parameter on the mass flow through the safety valve is to use the CATHARE-3 system-scale code to perform calculations on accidental transients. In this work, we have modelled an experiment, called “Cryostat Soupape”, to compare the pressure and temperature rise in the tank calculated by the code with experimental data. The aim is to evaluate the relevance of using CATHARE-3 before performing further calculations on industrial configurations.

4.2 Description of the Safety Valve modelling

CATHARE-3 has a specific sub-module named PIQSOUP that models a branch terminated by a safety valve (see Figure 13). Within this sub-module, it calculates the opening and the flow rate through the valve. The inputs are the opening pressure P_{set}, the maximum valve section S_{max}, the differential pressure ΔP necessary to obtain the full opening of the valve and the outside pressure P_{ext}.

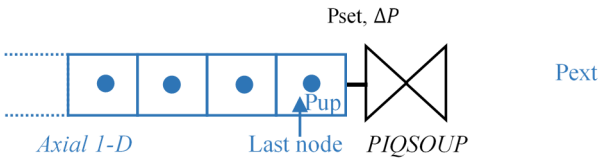

Figure 13 Description of the PIQSOUP sub-module

The valve opening is determined by an interpolation of the pressure gradient between 1 for the full opening and 0 for the closed valve. At each time step, the code computes the real pressure gradient between the upstream valve pressure P_{up} and the downstream pressure P'_{set}. As the PIQSOUP model exchanges mass with the outside, the downstream pressure P'_{set} is defined as the maximum between outside pressure P_{ext} and the opening pressure defined by the user P_{set}. This pressure gradient is thus compared with the differential pressure ΔP necessary to obtain the full opening of the valve and allows computing the opening rate S_r and the real section of the valve S_{tot}.

$$P'_{set} = \max(P_{ext}, P_{set}) \qquad (5)$$

$$P_{up} - P'_{set} \geq \Delta P \quad S_r = 1$$

$$0 < P_{up} - P'_{set} < \Delta P \quad S_r = \frac{P_{up} - P'_{set}}{\Delta P}$$

$$P_{up} - P'_{set} \leq 0 \quad S_r = 0$$

$$S_{tot} = S_{max} * S_r$$

With the valve opening section S_{tot}, the discharge mass flow can be calculated. To take into account sonic effect, its value is chosen as the minimum between the sonic and the subsonic flow rates. The subsonic flow rate $\dot{m}_{sub}$ is defined by:

$$\dot{m}_{sub} = S_{tot} * \sqrt{2 * \rho * (P_{up} - P_{ext})} \qquad (6)$$

The sonic flow rate $\dot{m}_{crit}$ is calculated with:

$$\dot{m}_{crit} = S_{tot} * \rho * v_s \qquad (7)$$

With ρ and v_s the density and the gas velocity at sonic condition determined with an iterative calculation using REFPROP described in [9]. Finally the mass flow $\dot{m}_{valve}$ through the valve is given by :

$$\dot{m}_{valve} = \min(\dot{m}_{sub}, \dot{m}_{crit}) \qquad (8)$$

4.3 Experimental validation on a tank discharge: Cryostat soupape experiment

4.3.1 Description of the Cryostat Soupape set up

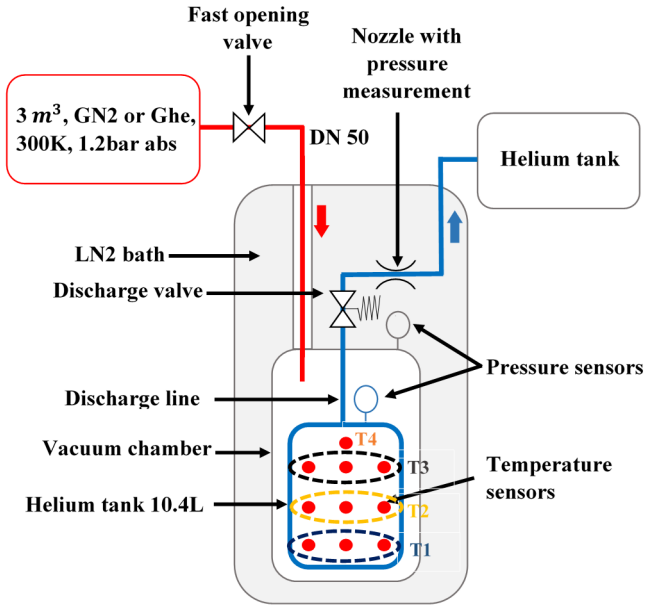

Figure 14 Schematic view of the Cryostat soupape experiment set up

The Cryostat Soupape is an experimental platform located at CEA Grenoble and used to perform estimations of the heat flux received by supercritical helium after a failure of the insulating vacuum [3]. The main dimensions of the test facility are given in Table 5. It is composed of a 10.4 L tank contained in a vacuum chamber thermally shielded by a liquid nitrogen bath to reduce radiation heat transfer (Figure 14). This tank is initially full of liquid helium at 4.2 K and 1 bar of pressure. A discharge line on the top of the tank goes through the vacuum chamber and the nitrogen bath to connect the tank and a discharge valve. This discharge valve is calibrated to open when the absolute pressure in the tank reaches 17 bar. A fast opening valve isolates the vacuum chamber from a pressurised nitrogen tank at 300K used to simulate the vacuum loss. At the opening of the valve, the hot nitrogen enters into the vacuum vessel by a line of 50mm diameter and condenses on the cold wall of the helium tank. Pressure and temperature inside the tank increase and helium becomes supercritical (P>2.2 bar and T>Tc=5.2 K). When the pressure in the tank is around 17 bars, the discharge valve opens and pressure remains constant during the remaining part of the transient.

Different sensors are distributed to follow the evolution of the physical conditions inside the tank. Three rows (T1, T2, T3) of three temperature sensors are placed at different heights in the tank. Another temperature sensor (T4) is located at the junction between the discharge line and the tank. Two pressure sensors measure pressure in the tank and in the vacuum chamber. A nozzle, equipped with two pressure probes, is placed just downstream of the discharge valve to determine the mass flow rate.

Component	Parameter	Value
Helium tank	Outer diameter	219.1 mm
	Inside diameter	211.6 mm
	Volume	10.4 L
	External Surface	2691 cm²
Discharge Line	Inner diameter pipes	[42.4 mm ... 13.9 mm]
	Length upstream the discharge valve	1.25 m
	Length in the vacuum chamber	1.2 m
	Total length	2.42 m
	Volume of the part between the discharge valve and the tank	0.42 L
Discharge valve	Calibrate opening pressure	17 bars

Table 5 Dimension of the main Cryostat Soupape components

4.3.2 *Evaluation of the heat flux during a loss of vacuum*

Two methods have been proposed by CEA for determining the heat flux received by the fluid [3] [27]. The first one is based on the first law of thermodynamics and on an internal energy balance before the discharge valve opening (closed system).

$$\varphi=\rho_i\times\frac{V}{S}\times\frac{\Delta U}{\Delta t} \quad \Delta U=U(P_f,\rho_i)-U(P_i,\rho_i) \qquad (9)$$

φ Heat flux received by helium (W/m²)
ρ_i Initial density (kg/m^3)
V Volume of the tank (m^3)
S Surface of the tank (m^2)
ΔU Internal energy variation between the final and the initial time (J)
Δt Time variation (s)
P_f, P_i Pressure at final and initial time (Pa)

In previous analyses based on experimental campaigns [3], the heat flux received by supercritical helium was estimated to be 1.85 W/m². A verification phase was carried out using heating resistors in the tank. The maximal difference between the heat flux injected by electrical resistors and the one measured using the first law of thermodynamic was +/-10%.

The second method involves measuring the mass flow through the discharge valve to determine the energy balance on an open system. If the system receives a heat power $\dot{Q}$ and discharges with constant pressure P, the mass flow $\dot{m}_{valve}$ through the discharge valve is determined by:

$$\dot{m}_{valve}=\frac{\dot{Q}}{h'} \qquad (10)$$

With $h'=v\left(\frac{\partial h}{\partial v}\right)_P$ (11)

With this expression, it is possible to calculate analytically the required mass flow rate $\dot{m}_{valve}$ so that the pressure remains constant. This value depends on the heat power received by the fluid $\dot{Q}$ and $\left(\frac{\partial h}{\partial v}\right)_P$, the partial derivative of the enthalpy h with respect to the specific volume v at constant pressure [27]. This mass flow rate can be compared with the one computed by CATHARE-3.

4.3.3 *Model description of the Cryostat Soupape*

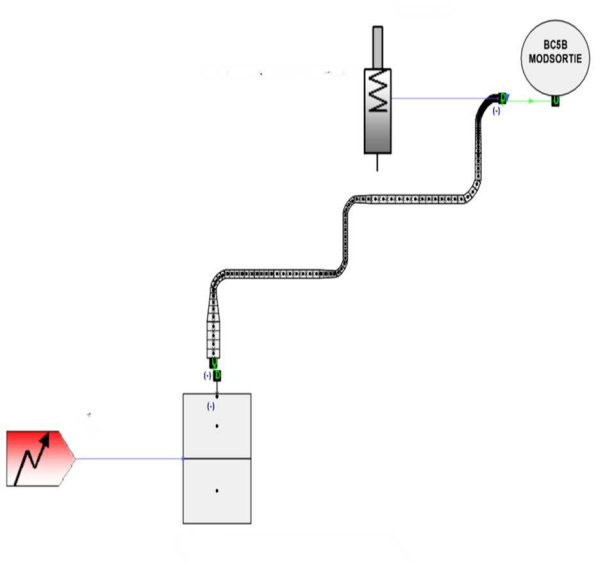

Figure 15 CATHARE-3 model of the Cryostat Soupape experiment

It was chosen to only consider the part of the discharge line upstream of the discharge valve. As shown in Figure 15, the data set describes the tank with a 0-D module. This volume is linked to a 1-D pipe (160 meshes) which represents the discharge line. According to recommendations made for space discretisation in CATHARE models, the length ratio between two consecutive nodes should be between 0.8 and 1.2 and the last node before the component used to model the discharge valve has to be lower than 1 mm. The mesh size is here decreased by a ratio between 0.85 and 0.97 near the discharge valve, so that the last mesh is less than 1 mm long. The number of mesh has been chosen to be sufficient to insure the convergence of the calculation. We consider no singular loss along the discharge line or at the junction between the tank and the line. Only vertical bends are represented to take into account gravity effects. The PIQSOUP sub-module is used to model the discharge valve with the input values given in Table 6. As the line downstream of the discharge valve is not taken into account, the external pressure is fixed to 1 bar.

Parameter	Value
Opening pressure P_{tar}	17 bars
Maximal opening section S_{max}	19.63 mm²
Differential pressure for the maximum opening ΔP	1 bar

Table 6 Parameters of the PIQSOUP used to model the discharge valve

As the major part of the discharge canal upstream of the valve is inside the vacuum chamber, there is no thermal exchange between the line and the liquid nitrogen at 77K. Moreover, the power deposited on the discharge line is small compared to the power received by helium in the tank, so the line in the CATHARE-3 model is assumed adiabatic. The heat flux is transferred directly to the fluid. The total power injected is 4978 W which corresponds to the value of 1.85 W/cm² measured during the experimental campaign

As CATHARE-3 is not able to model two-phase helium flow, the code calculation starts from the first experimental point when helium is supercritical in the entire tank. The initial conditions of the transient are a pressure of 6.19 bars and a temperature of 6.01 K, according to the pressure and the mean temperature measured experimentally at t = 1.53 s. As the transient begins from a steady state, stratification effects before t = 1.53 s are not considered. This hypothesis is acceptable for the tank due to the 0-D modelling, but temperature and density stratification in the discharge line are not taken into account in the initial state. The heat flux is imposed in the model from t = 1.53 s until the end of the transient.

4.3.4 Pressure and temperature increase in the tank

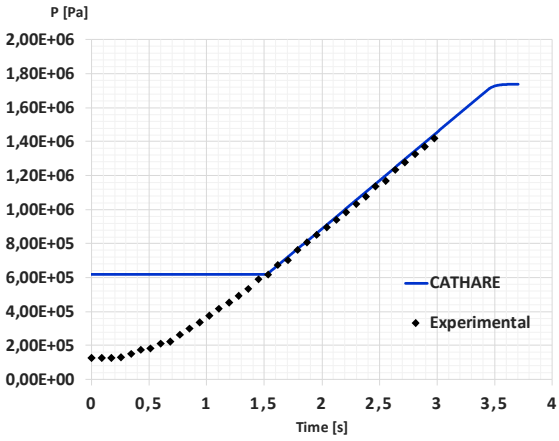

Figure 16 Helium pressure increase in the tank of the Cryostat Soupape

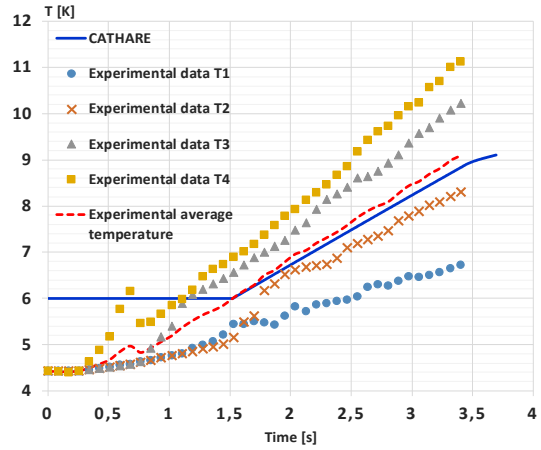

Figure 17 Helium temperature increase in the tank of the Cryostat Soupape

The loss of insulating vacuum can be divided in two distinct phases. The first one is the helium pressure and temperature increase in a closed system before the discharge valve opening. Once the valve opens, the second phase starts with the transition from a closed system to an open one. Figure 16 and Figure 17 show respectively the pressure and the temperature increase calculated by CATHARE-3 and measured experimentally before the discharge valve opening. The temperature T4 is measured by only one temperature sensor, whereas T1,T2 and T3 are average values of temperatures measured by three sensors at the same height. The time before 1.53s correspond to two-phase helium in the tank and is not modelled with CATHARE-3. According to experimental data, the critical pressure is reached in 0.68s, but at this moment a large part of the fluid in the tank is colder than the critical temperature. Despite the low height of the tank, it is observed experimentally that heat stratification occurs quickly after the beginning of the loss of insulating vacuum. After 1.53s, all the fluid is in supercritical phase and the 1.85W/cm² heat flux is applied in the CATHARE-3 model. The pressure increase before the valve opening calculated by the code follows quite well the measured one with a maximal relative error of 2.4%. The temperature increases a little slower in the simulation compared to the experimental average temperatures but the two slopes are similar. The maximal relative difference on the average temperature is 3%. It could be explained by fact that the CATHARE-3 model do not consider stratification effects. Indeed, when the heat flux injection starts, the experimental temperature difference between the bottom and the top of the tank is already 1.44 K. This stratification appears also in the discharge line due to mass transfer between the two volumes. Moreover, the experimental average temperature compared with CATHARE-3 calculation is not completely representative as it is calculated with a limited numbers of local measurements.

4.3.5 Mass flow rate calculation

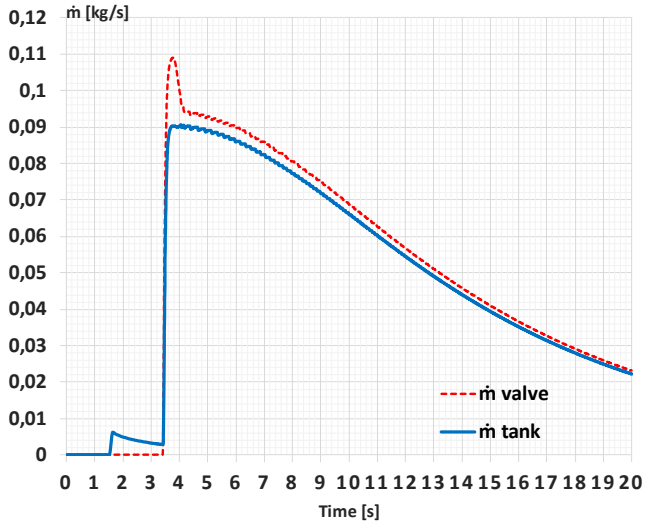

Figure 18 Mass flows calculated by CATHARE at the junction of the tank and the discharge valve ($\dot{m}_{tank}$) and through the discharge valve ($\dot{m}_{valve}$)

Figure 19 Localisation of the mass flows computed by CATHARE

Mass flows at the inlet and outlet of the discharge line have been calculated with CATHARE-3 (respectively $\dot{m}_{tank}$ and $\dot{m}_{valve}$). The two quantities are represented on the Figure 18 and their localisations are given by Figure 19. CATHARE-3's calculation of $\dot{m}_{tank}$ confirms that mass transfer takes place between the tank and the adiabatic discharge line before the valve opening. The discharge valve is closed until t = 3.42s. Before this time, hot helium from the tank moves in the discharge line, which explained the positive value of $\dot{m}_{tank}$ between the beginning of the heat flux injection and the opening of the discharge valve. After the opening of the discharge valve, the pressure in the tank remains almost constant at 17.4 bars. During first seconds after the beginning of the discharge, a difference can be observed between the two mass flows with a peak of $\dot{m}_{valve}$. This peak is physically valid as part of the adiabatic line hypothesis. Indeed, due to the mass transfer observed between the tank and the discharge line at the beginning of the transient, the cold helium initially present in the line is adiabatically compressed by warmer helium from the tank. As the pressure is similar in the tank and along the pipe (fluid velocity is small during the pressure increase so there is no pressure loss due to friction), the temperature stratification involves a density stratification. The peak of $\dot{m}_{valve}$ is thus due to the discharge of this cold and dense volume of helium. This difference was expected but CATHARE-3 reveals that this effect is not negligible. The maximal difference on the mass flows reaches 21% even if the volume ratio between the line and the tank is small (4%). For the remaining of the transient scenario, the two mass flows have similar evolutions with small differences due to pressure loss. With a pressure of 17.4 bars and a 1.85W/cm² heat flux, the analytical model (10) give a 0.084 kg/s mass flow at the discharge valve opening. This value is very close to $\dot{m}_{tank}$ = 0.090 kg/s calculated by CATHARE-3.

4.4 Conclusion on the Cryostat Soupape Experiment

The modelling of the Cryostat Soupape experiment with CATHARE-3 gives the opportunity to evaluate the abilities of the code to simulate the pressure and temperature increase in a small supercritical helium tank with an input heat flux of 1.85 W/cm². In these conditions, the code gives results close to experimental data with coherent pressure and temperature evolutions. The assumption made on the choice of initial conditions with supercritical helium does not affect the relevance of the results. The discharge mass flow at the junction between the discharge line and the tank has also been compared with the result of an energy balance on an open system. For this configuration, CATHARE-3 seems to be reliable to model the helium discharge phenomenon.

The code shows that in the presence of an adiabatic discharge line between the vessel to be protected and the discharge valve, mass transfer and density stratification phenomena can lead to higher mass flow through the discharge valve than the mass flow at the tank outlet. CATHARE-3 gives a first estimation of this phenomenon which is not negligible even if the volume of the line is small compared to the volume of the tank (4%).

Perspectives for future modelling could be further calculations on a tank and a discharge line with different geometries, representative to industrial installations where the discharge line volume could be larger. It seems also necessary to study the case with a heat flux deposited on the discharge line, which will affect the density stratification and hence the mass flow rate at discharge valve.

5 General conclusion and perspectives

This work has shown the abilities of CATHARE-3 to perform calculations of accidental transients on different cryogenic devices used in tokamak reactors. Two safety issues on cryogenic components have been explored, with a first study of thermal-hydraulic calculations in superconducting cables (CICC) and a second study of a supercritical helium discharge. Additional correlations adapted for helium and superconducting cable were implemented and the modular structure of the code allows representing all the thermal and hydraulic components of these cryogenic systems. The code gives consistent results with experimental data and with calculations performed with THEA, the actual reference code for the modelling of superconducting magnets. With these first evaluations and its abilities to model severe transients in various cryogenic set-ups, CATHARE-3 appears to be an efficient and a reliable simulation tool for accidental analysis.

Short-term outlook is pursuing the validation of the code with a dedicated experimental support. One specific Separate Effect Test which has been foreseen is to have an experimental set up to perform measurements of heat flux received by a supercritical helium flow in a pipe in case of loss of isolating vacuum. These tests would be necessary to validate CATHARE-3 predictions on this configuration and could provide new correlations for the modelling of cryogenic discharge lines. Further investigations of quench scenarios in TFC JT-60SA need to be performed to continue the evaluation of CATHARE-3 abilities in more realistic cases. In a first approximation, the electrical current transportation would not be considered, so only representative heat load deposition would be determined with THEA calculation. Finally, the two studies could be combined with the modelling of the superconducting magnets, the quench line and the helium recovery system (quench tank) to address the quench scenario including all the cryogenic components

Long-term outlook is the implementation of electrical laws in the code to model quench cases with all the couplings between physical phenomena (electro-magnetism and thermal hydraulics) in a superconducting magnet. The conclusion of these developments will need to be validated with experimental data on a dedicated set up.

6 References

[1] F. Barre and M. Bernard, “The CATHARE code strategy and assessment,” *Nuclear Engineering and Design,* no. 124, pp. 257 - 284, 1990.

[2] L. Bottura, C. Rosso and M. Breschi, “A general model for thermal, hydraulic and electric analysis of superconducting cables,” *Cryogenics,* vol. 40, pp. 617-626, 2000.

[3] E. Ercolani, A. Gauthier, P. Gully and J. M. Poncet, “Quantification of heat flux in supercritical helium,” 2016. [Online]. Available: https://indico.cern.ch/event/495194/contributions/2181322/attachments/1340321/2018199/seminaire_cryost_soup_cern.pdf.

[4] P. Emonot, A. Souyri, J. L. Gandrille and F. Barré, “CATHARE-3: A new system code for thermal-hydraulics in the context of the NEPTUNE project,” *Nuclear Engineering and Design,* vol. 241, pp. 4476-4481, 2011.

[5] M. Ishii, Thermo-fluid dynamic theory of two-phase flow, Eyrolles, 1975.

[6] D. Bestion, “The physical closure laws in the CATHARE code,” *Nuclear Engineering and Design,* no. 124, pp. 229-245, 1990.

[7] D. Bestion, F. Barre and B. Faydide, “Methodology, status and plans for development and assessment of CATHARE code,” in *OECD/CSNI*, Annapolis, USA , 5th-8th November 1996.

[8] F. Barre, M. Parent and B. Brun, “Advanced numerical methods for thermalhydraulics,” *Nuclear Engineering and Design,* vol. 145, pp. 147-158, 1993.

[9] G. Mauger, N. Tauveron, F. Bentivoglio and A. Ruby, “On the dynamic modeling of Brayton cycle power conversion systems with the CATHARE-3 code,” pp. 1002-10016, 2019.

[10] E. W. Lemmon, M. L. Huber and M. O. McLinden, "NIST Standard Reference Database 23: Reference Fluid Thermodynamic and Transport Properties-REFPROP Version 9.1," National Institute of Standards and Technology, Standard Reference Data Program, Gaithersburg, 2013.

[11] V. Tomarchio, P. Barabaschi, A. Cucchiaro, P. Decool, A. Della Corte, A. Di Zenobio, D. Duglue, L. Meunier, L. Muzzi, M. Nannini, M. Peyrot, G. Phillips, A. Pizzuto, C. Portafaix, L. Reccia, K. Yoshida and L. Zani, "Design of the JT-60SA Superconducting Toroidal Field Magnet," *IEEE TRANSACTIONS ON APPLIED SUPERCONDUCTIVITY,* vol. 20, no. 3, 2010.

[12] L. Zani, P. Barabaschi and E. Di Pietro, "Status of European manufacture of Toroidal Field conductor and strand for JT-60SA project," *Fusion Engineering and Design,* no. 88, pp. 555-558, 2012.

[13] M. Bagnasco, L. Bottura and M. Lewandowska, "Friction factor correlation for CICC's based on a porous media analogy," *Cryogenics,* vol. 50, pp. 711-719, 2010.

[14] P. Decool, H. Cloez, G. Gros, G. Jiolat, J. L. Maréchal, A. Torre and J. M. Verger, "CEA studies and qualifications prior to the JT-60SA TF coils manufacture," *Fusion Engineering and Design,* vol. 88, pp. 1627-1630, 2013.

[15] P. Decool, H. Cloez, G. Jiolat, M. Tena, L. Zani, C. Hoa, W. Abdel Maksoud and M. Verrechia, "JT-60SA TF Coils: Experimental Check of Hydraulic Operating Conditions," *IEEE TRANSACTIONS ON APPLIED SUPERCONDUCTIVITY,* vol. 26, no. 4, 2016.

[16] S. Nicollet, D. Ciazynski, J. L. Duchateau, B. Lacroix and B. Renard, "Evaluation of the ITER Cable In Conduit Conductor heat transfer," *Elsevier Ltd, Beijing, China,* pp. 589-592, 2005.

[17] W. Abdel Maksoud, P. Bargueden, A. Bouty, G. .Dispau, A. Donati, D. Eppelle, L. Genini, P. Guiho, Q. Guihard, J. M. Joubert, O. Kuster, D. Médioni, F. Molinié, A. Sinanna, N. Solenne, S. Somson and L. Vieillard, "Status of the cold test facility for the JT-60SA tokamak toroidal field coils," *Fusion Engineering and Design,* pp. 208-211, 2015.

[18] W. Abdel Maksoud, L. Genini, D. Ciazynski, P. Decool, Y. Huang, S. Nicollet and A. Torre, "Results of the first JT-60SA toroidal field coils tests in the cold test facility," *Fusion Engineering and Design,* vol. 124, pp. 14-17, 2017.

[19] W. Abdel Maksoud, L. .Genini, D. Ciazynski, Y. Huang and L. Vieillard, "Progress of the JT-60SA Toroidal Field Coils Tests in the Cold Test Facility," *IEEE TRANSACTIONS ON APPLIED SUPERCONDUCTIVITY,* vol. 28, no. 3, 2018.

[20] Y. Huang, W. Abdel Maksoud, L. Genini, D. Ciazynski, P. Decool and A. Torre, "Quench tests analysis of first the JT-60SA toroidal field coils," *Fusion Engineering Design,* vol. 124, pp. 147-152, 2017.

[21] Y. Huang, "Study and modelling of the thermohydraulic phenomena taking place during the quench of a superconducting magnet cooled with supercritical helium," 2018. [Online]. Available: https://tel.archives-ouvertes.fr/tel-01912703.

[22] Y. Huang, W. Abdel Maksoud, B. Baudouy, D. Ciazynski, P. Decool, L. Genini, B. Lacroix, Q. Le Coz, S. Nicollet, F. Nunio, A. Torre, R. Vallcorba and L. Zani, "Numerical Modeling of the Quench Propagation Phase in the JT-60SA TF Coils," *IEEE Transaction on Applied Superconductivity,* vol. 28, no. 3, 2018.

[23] S. Nicollet, W. Abdel Maksoud, J. Cazabonne, D. Ciazynski, P. Decool, Y. Huang, B. Lacroix, A. Torre and L. Zani, "Parametric Analyses of JT-60SA TF Coils in the Cold Test Facility With SuperMagnet Code," *IEEE Transactions on applied superconductivity,* vol. 28, no. 3, 2018.

[24] Q. Le Coz, D. Ciazynski, B. Lacroix, S. Nicollet, F. Nunio, A. Torre, R. Vallcorba and L. Zani, "Towards a multi-physic platform for fusion magnet design. Application to DEMO TF coil.," *Fusion Engineering and Design,* vol. 124, pp. 104-109, 2017.

[25] W. Lehmann and G. Zahn, "Safety Aspects for LHe Cryostat and LHe Transport Containers," IPC Science and Technology Press, London, 1978..

[26] C. Zoller, "Experimental Investigation and Modelling of Incidents in Liquid Helium Cryostats," Karlsruher Instituts für

Technologie, 2018.

[27] E. Ercolani, P. Gully, C. Meuris, J. M. Poncet and L. Miquet, “Safety in cryogenics EBE914,” Technique de l'ingénieur, 2015.